


## Theoretical study of evaporation-residue cross sections of superheavy nuclei

Xing-Jian Lv (吕行健), Zi-Yang Yue (岳子洋), Wei-Juan Zhao (赵维娟), and Bing Wang (王兵)<sup>\*</sup>  
*School of Physics and Microelectronics, Zhengzhou University, Zhengzhou 450001, China*

 (Received 29 April 2021; accepted 16 June 2021; published 28 June 2021)

Based on the empirical coupled-channel model for calculating capture cross section and the statistical model for calculating survival probability, we propose an analytical formula for describing the fusion probability. The cold-fusion and hot-fusion reactions leading to superheavy nuclei have been systematically investigated. For both the cold-fusion and hot-fusion reactions, the measured evaporation-residual (ER) cross sections can be reproduced acceptably well by using the formula with the same parameter set. Simultaneously, the ER cross sections for some reactions producing elements  $Z = 119$  and  $120$  are studied. It is found that the projectile-target combinations  $^{50}\text{Ti} + ^{249}\text{Bk}$  and  $^{50}\text{Ti} + ^{249,251}\text{Cf}$  are considered as the most promising reactions for the syntheses of the next two superheavy elements beyond Og. The maximal ER cross section for  $^{50}\text{Ti} + ^{249}\text{Bk}$  is 48.2 fb at the incident energy  $E_{c.m.} = 226$  MeV. For  $^{50}\text{Ti} + ^{249,251}\text{Cf}$ , the maximal ER cross section is about 10 fb at the incident energies around  $E_{c.m.} = 232$  MeV.

DOI: [10.1103/PhysRevC.103.064616](https://doi.org/10.1103/PhysRevC.103.064616)

### I. INTRODUCTION

In recent decades, the synthesis of superheavy elements (SHEs) has been at the frontier of modern nuclear physics [1]. Elucidating the nuclear and chemical properties of SHEs is a fundamental quest in nuclear physics and chemistry. Up to now, 118 chemical elements are known and fill the periodic table of the elements to the end of the seventh row. SHEs with  $Z \leq 118$  have been synthesized via cold-fusion reactions with Pb and Bi as targets [1,2] and hot-fusion reactions with  $^{48}\text{Ca}$  as projectiles [3,4]. SHEs beyond oganesson (Og,  $Z = 118$ ) will start the eighth row of the periodic table. However, there are many experimental challenges in the synthesis of SHEs beyond Og. For example, projectiles heavier than  $^{48}\text{Ca}$  are needed in fusion-evaporation reactions because of insufficient amounts of materials of elements with proton numbers  $Z > 98$  as targets. The reactions  $^{50}\text{Ti} + ^{249}\text{Bk}$  and  $^{249}\text{Cf}$  [5],  $^{54}\text{Cr} + ^{248}\text{Cm}$  [6],  $^{58}\text{Fe} + ^{244}\text{Pu}$  [7], and  $^{64}\text{Ni} + ^{238}\text{U}$  [8] have already been examined for the synthesis of SHEs with  $Z = 119$  and  $120$ . However, none of these experiments provide evidence for the synthesis of the new elements.

The evaporation-residue (ER) cross section  $\sigma_{\text{ER}}$  of the superheavy nuclei (SHN) produced via fusion-evaporation reactions depends strongly on the projectile-target combination and the incident energy. Hence, the theoretical study of such dependencies is useful particularly for guiding future experimental searches as  $\sigma_{\text{ER}}$  of the produced SHN are tiny. For example, the optimal incident energy and the maximal  $\sigma_{\text{ER}}$  of the synthesis of elements 119 and 120 with  $^{50}\text{Ti}$  as the projectile have been investigated extensively [9–14].

The fusion-evaporation reaction process producing SHN is divided into three reaction stages, namely the capture process,

the fusion process, and the de-excitation of the excited compound nucleus (CN) against fission. Accordingly, the  $\sigma_{\text{ER}}$  is calculated as the summation over all partial waves  $J$  of the three-term expression

$$\sigma_{\text{ER}}(E_{c.m.}) = \sum_J \sigma_{\text{capture}}(E_{c.m.}, J) P_{\text{CN}}(E_{c.m.}, J) \times W_{\text{sur}}(E_{c.m.}, J), \quad (1)$$

where  $\sigma_{\text{capture}}$  is the capture cross section for the transition of the colliding nuclei over the entrance (Coulomb) barrier,  $P_{\text{CN}}$  is the fusion probability for describing the competition between complete fusion and quasifission, and  $W_{\text{sur}}$  is the survival probability of the excited CN.  $E_{c.m.}$  is the incident energy in the center-of-mass frame. In the description of the capture and the de-excitation stages, most theoretical approaches for the formation of SHN have a similar viewpoint [12,15–25]. Usually  $P_{\text{CN}}$  is calculated by some models [12,15–17,25–28] or by empirical formulas [9–11,19,20,29,30]. However, there are some serious ambiguities in the reaction mechanism of fusion dynamics [31,32]. Hence, a number of theoretical calculations of the ER cross sections for the synthesized SHN show remarkable agreement with the measured data, while if one focuses on the theoretical values of  $P_{\text{CN}}$ , it can be found that the calculated values differ by two or three orders of magnitude [11,31,33]. In this sense, the predictive power of these models remains quite limited in giving the maximal  $\sigma_{\text{ER}}$  for new SHN synthesis. For example,  $\sigma_{\text{ER}}$  for the  $3n$  emission channel of the reaction  $^{50}\text{Ti} + ^{249}\text{Cf}$  ranges from 1.5 fb to 760 fb [34].

Therefore, it is very important to examine carefully these three steps in the study of the synthesis mechanism of SHN. Recently, based on a large number of the measured capture excitation functions of light and medium-heavy systems, we have developed an empirical coupled-channel (ECC) model

<sup>\*</sup>bingwang@zzu.edu.cn

and performed a systematic study for calculating the capture excitation functions for 220 reaction systems [35]. In this ECC model, the effects of couplings to inelastic excitations and neutron transfer channels are effectively taken into account by introducing an empirical barrier distribution function [35–37]. In addition, based on the present ECC model, for reactions with quasifission barrier high enough ( $P_{\text{CN}} \approx 1$ ) [38], the measured ER cross sections have been used to constrain the key parameters in the statistical model for calculating  $W_{\text{sur}}$  [39]. The measured ER cross sections of 48 fusion-fission reactions are systematically well reproduced. In the present work, based on our previous work on capture and survival processes, we propose an analytical formula for a systematic description of the fusion probability in reactions producing SHN. Then the cold-fusion and hot-fusion reactions leading to SHN will be further systematically investigated. Finally, we will give the predictions for the ER cross sections of SHN with  $Z = 119$  and 120.

The paper is organized as follows. In Sec. II, we introduce the ECC model to calculate the capture cross section, the empirical formula for describing the fusion probability, and the statistical model to calculate the survival probability. The cold-fusion reactions and the hot-fusion reactions leading to SHN will be systematically investigated in Sec. III where the predictions of the ER cross sections of SHN with  $Z = 119$  and 120 will be given. Finally, a summary is given in Sec. IV.

## II. CALCULATIONAL METHODS

### A. Capture cross section and the ECC model

The capture cross section at a given center-of-mass energy  $E_{\text{c.m.}}$  can be calculated as the sum of the cross section for each partial wave  $J$ ,

$$\sigma_{\text{capture}}(E_{\text{c.m.}}) = \frac{\pi \hbar^2}{2\mu E_{\text{c.m.}}} \sum_{J=0}^{J_{\text{max}}} (2J+1) T(E_{\text{c.m.}}, J), \quad (2)$$

where  $\mu$  is the reduced mass of the reaction system.  $T$  denotes the penetration probability of the potential barrier between colliding nuclei at a given  $J$ .  $J_{\text{max}}$  is the critical angular momentum: For a partial wave with angular momentum larger than  $J_{\text{max}}$ , the ‘‘pocket’’ of the interaction potential disappears.

Within the ECC model, the penetration probability  $T$  in Eq. (2) is calculated as [35–37]

$$T(E_{\text{c.m.}}, J) = \int f(B) T_{\text{B}}(E_{\text{c.m.}}, J, B) dB, \quad (3)$$

with  $B$  being the barrier height. Here the coupled-channel effects are effectively taken into account by introducing a barrier distribution function  $f(B)$  [35]. When the interaction potential around the Coulomb barrier is approximated by an ‘‘inverted’’ parabola, the well-known Hill-Wheeler formula [40] can be adopted to calculate the penetration probability, which is written as

$$T_{\text{B}}^{\text{HW}}(E_{\text{c.m.}}, J, B) = \left\{ 1 + \exp \left[ \frac{2\pi}{\hbar\omega(J)} \left( \frac{\hbar^2 J(J+1)}{2\mu R_{\text{B}}^2(J)} + B - E_{\text{c.m.}} \right) \right] \right\}^{-1}, \quad (4)$$

where  $R_{\text{B}}(J)$  and  $\hbar\omega(J)$  are the position of the barrier and the curvature for the  $J$ th partial wave, respectively.

Note that for light systems at sub-barrier energies and heavy systems at deep sub-barrier energies, the parabolic approximation is not appropriate due to the omitting of the long tail of the Coulomb potential [41]. Therefore, in these cases, the Hill-Wheeler formula does not describe properly the behavior of capture cross sections at the corresponding energy region. In the present work, we are dealing with energies near and above the Coulomb barrier, an energy region where the Hill-Wheeler formula can be applied.

In our ECC model, the barrier distribution function  $f(B)$  is taken to be an asymmetric Gaussian function

$$f(B) = \frac{1}{N} \begin{cases} \exp \left[ -\left( \frac{B-B_{\text{m}}}{\Delta_1} \right)^2 \right], & B < B_{\text{m}}, \\ \exp \left[ -\left( \frac{B-B_{\text{m}}}{\Delta_2} \right)^2 \right], & B > B_{\text{m}}. \end{cases} \quad (5)$$

$f(B)$  satisfies the normalization condition  $\int f(B) dB = 1$ . The normalization coefficient  $N = \sqrt{\pi}(\Delta_1 + \Delta_2)/2$ .  $\Delta_1$ ,  $\Delta_2$ , and  $B_{\text{m}}$  denote the left width, the right width, and the most probable value of barrier distribution function, respectively. In our ECC model, the barrier distribution is related to the couplings to low-lying collective vibrational states, rotational states, and positive  $Q$ -value neutron transfer channels. For calculating these three parameters of the barrier distribution function, empirical formulas were proposed by performing a systematic study for calculating the capture excitation functions of 220 reaction systems [35]. In addition, this ECC model has been extended to describe the complete fusion cross sections for reactions involving weakly bound nuclei at energies above the Coulomb barrier [42,43]. More details for the present ECC model can be found in Refs. [35,43].

### B. Empirical formula for calculating the fusion probability

As mentioned above, the fusion probability  $P_{\text{CN}}$  is more unclear because of some serious ambiguities in the reaction mechanism of fusion dynamics. In addition, the influence of quasifission barrier  $B_{\text{qf}}$  on fusion has been discussed a lot [10,11,29,30,44]. For the cold-fusion reactions, it is found that the maximal ER cross section of the  $1n$  channel as well as the calculated  $P_{\text{CN}}$  decrease exponentially with increasing the charge number  $Z_{\text{CN}}$  of the CN [33]. Moreover, a good linear relation holds between the  $B_{\text{qf}}$  and the  $Z_{\text{CN}}$ , which is shown in Fig. 1. Hence, we expect that the  $P_{\text{CN}}$  decreases with decreasing quasifission barrier height and the excitation energy  $E_{\text{CN}}^*$  ( $E_{\text{CN}}^* = E_{\text{c.m.}} + Q$ , with  $Q$  being the reaction energy) of the CN. Furthermore, if the quasifission barrier high enough, the  $P_{\text{CN}}$  should be close to 1. Then we propose an analytical formula for describing the fusion probability  $P_{\text{CN}}$ , which reads

$$P_{\text{CN}} = \frac{1}{1 + \exp(C_0|\eta|Z_{\text{CN}} - C_1 B_{\text{qf}} - 0.05 E_{\text{CN}}^*)}, \quad (6)$$

where  $\eta = (A_1 - A_2)/(A_1 + A_2)$  is the mass asymmetry of the reaction system with  $A_1$  and  $A_2$  being the mass numbers of projectile and target. The excitation energy  $E_{\text{CN}}^*$  is in the unit of MeV.  $C_0$  and  $C_1$  are two constants. In addition, when the quasifission barrier height is close to zero, the  $P_{\text{CN}}$  should be

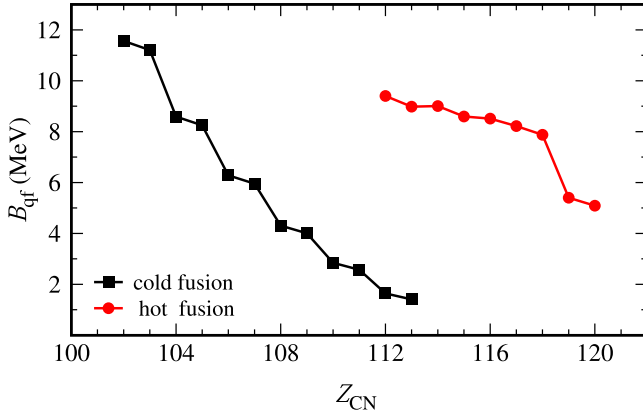


FIG. 1. Quasifission barrier height  $B_{qf}$  for the cold-fusion reactions (solid squares) and the hot-fusion reactions (solid circles) as a function of the charge number  $Z_{CN}$  of the SHN. For the produced SHN with  $Z_{CN} = 119$  and  $120$ , the  $B_{qf}$  are of the reactions  $^{50}\text{Ti} + ^{249}\text{Bk}$  and  $^{50}\text{Ti} + ^{249}\text{Cf}$ , respectively.

also close to zero. Considering this physical limit, we add a factor  $\exp(C_2/B_{qf})$  to  $C_0$  and the constant  $C_2$  should be small. Then  $C_0$  becomes  $C_0 \exp(C_2/B_{qf})$ . The constants  $C_0 = 0.23$ ,  $C_1 = 1.2 \text{ MeV}^{-1}$ , and  $C_2 = 0.6 \text{ MeV}$  are obtained by fitting the ER cross sections of  $^{50}\text{Ti} + ^{209}\text{Bi}$ ,  $^{58}\text{Fe} + ^{208}\text{Pb}$ ,  $^{64}\text{Ni} + ^{208}\text{Pb}$ , and  $^{70}\text{Zn} + ^{208}\text{Pb}$ .

### C. Survival probability of a compound nucleus

An excited CN can decay via emitting photon(s), neutron(s), proton(s), or light-charged particle(s) like  $\alpha$  particle or via fission. For the superheavy compound nuclei, the widths for emission of light-charged particle(s) are much less than the width for neutron emission  $\Gamma_n$  owing to the high Coulomb barrier for the emission of charged particles. Furthermore, the photon-emission channel only competes with other processes when excitation energy is smaller than the neutron binding energy and therefore is disregarded [45,46]. Hence the survival probability under the evaporation of  $x$  neutron(s) is calculated as follows [47]:

$$W_{\text{sur}}(E_{\text{CN}}^*, x, J) = P_{\text{xn}}(E_{\text{CN}}^*) \prod_{i=1}^x \frac{\Gamma_n(E_i^*, J)}{\Gamma_n(E_i^*, J) + \Gamma_f(E_i^*, J)}, \quad (7)$$

where  $i$  is the index of the evaporation step,  $P_{\text{xn}}$  is the probability of realization of an  $xn$  channel at the initial excitation energy  $E_{\text{CN}}^*$  of the CN,  $\Gamma_f$  is the fission width, and  $E_i^*$  is the excitation energy before evaporating the  $i$ th neutron.

The width of neutron-evaporation channel  $\Gamma_n$  is given as [48]

$$\Gamma_n(E_i^*, J) = \frac{2m_n R^2}{\pi \hbar^2 \rho(E_i^*, J)} \int_0^{E_i^* - B_n} \varepsilon \rho_d(E_i^* - B_n - \varepsilon, J) d\varepsilon. \quad (8)$$

Here  $m_n$  is the neutron mass and  $R$  is the radius of the nucleus before evaporating the  $i$ th neutron.  $\rho$  is the level density of the decaying nucleus and  $\rho_d$  denotes the level density of the residue nucleus after the neutron emission.  $\varepsilon$  denotes the

kinetic energy of the emitted neutron.  $B_n$  denotes the binding energy of the emitted neutron with the residue nucleus.

The fission width can be calculated with the Bohr-Wheeler formula [49] as

$$\Gamma_f(E_i^*, J) = \frac{1}{2\pi \rho(E_i^*, J)} \int_{-B_f}^{E_i^* - B_f} \frac{\rho_{\text{sd}}(E_i^* - B_f - \varepsilon, J)}{1 + \exp[-2\pi \varepsilon / \hbar \omega]} d\varepsilon, \quad (9)$$

where  $\rho_{\text{sd}}$  is the level density at the saddle point.  $\hbar \omega$  denotes the curvature of the fission barrier and is taken to be  $2.2 \text{ MeV}$  [27,50,51]. The fission barrier  $B_f$  consists of a macroscopic liquid-drop component and a microscopic shell correction energy including the washing out effect, which is written as [27,47,51]

$$B_f = B_f^{\text{mac}} + B_f^{\text{mic}} \exp(-E^*/E_d), \quad (10)$$

with  $E_d$  being the shell damping energy, taken to be  $18.5 \text{ MeV}$  [52]. The macroscopic component  $B_f^{\text{mac}}$  is described with the liquid-drop model [53,54]. The shell correction energy  $B_f^{\text{mic}}$  is calculated by the Weizsäcker-Skyrme (WS) mass formula [55,56].

The level density is calculated with the Fermi-gas model [27] as

$$\rho(E^*, J) = \frac{2J + 1}{24\sqrt{2}\sigma^3 a^{1/4} (E^* - \delta)^{5/4}} \times \exp\left[2\sqrt{a(E^* - \delta)} - \frac{(J + 1/2)^2}{2\sigma^2}\right], \quad (11)$$

where  $\sigma^2 = 6\bar{m}^2 \sqrt{a(E^* - \delta)}/\pi^2$  and the average projection of the angular momentum of single particle states at Fermi surface  $\bar{m}^2 \approx 0.24A^{2/3}$ . The pairing correction  $\delta$  is set to be  $-12/\sqrt{A} \text{ MeV}$ ,  $0$ , and  $12/\sqrt{A} \text{ MeV}$  for odd-odd, even-odd, and even-even nuclei, respectively.

In the present work, the level density parameter  $a$  taking into account the volume, surface, and curvature dependence of the single-particle level density at the Fermi surface is adopted and given by [52]

$$a = 0.04543r_0^3 A + 0.1355r_0^2 A^{2/3} B_s + 0.1426r_0 A^{1/3} B_k, \quad (12)$$

with  $B_s$  and  $B_k$  being the surface and curvature factors defined in the droplet model [54].  $r_0$  is the radius parameter, which is set to  $1.16 \text{ fm}$ . For neutron-evaporation channels,  $B_s$  and  $B_k$  are taken to be  $1$ . For the fission channel,  $a_f$  is calculated by the formulas proposed in Ref. [39].

In the case of  $1n$  emission channel, the probability of realization is given as

$$P_{1n}(E_{\text{CN}}^*) = \exp[-(E_{\text{CN}}^* - B_n - 2T)^2/2\Sigma^2], \quad (13)$$

where  $T = [1 + \sqrt{1 + 4aE_{\text{CN}}^*}]/2a$  is the temperature of the nucleus and the width of excitation function  $\Sigma$  is taken to be  $2.5 \text{ MeV}$ . For other cases ( $x > 1$ ), the probability of realization is given by the formula proposed by Jackson [57],

$$P_{\text{xn}}(E_{\text{CN}}^*) = I(\Delta_x, 2x - 3) - I(\Delta_{x+1}, 2x - 1). \quad (14)$$

Here,  $I(z, m) = \frac{1}{m!} \int_0^z u^m e^{-u} du$  is the Pearson's incomplete gamma function,  $\Delta_x = [E_{\text{CN}}^* - \sum_{i=1}^x B_n(i)]/T$ , where  $B_n(i)$  is the separation energy of the  $i$ th evaporated neutron.

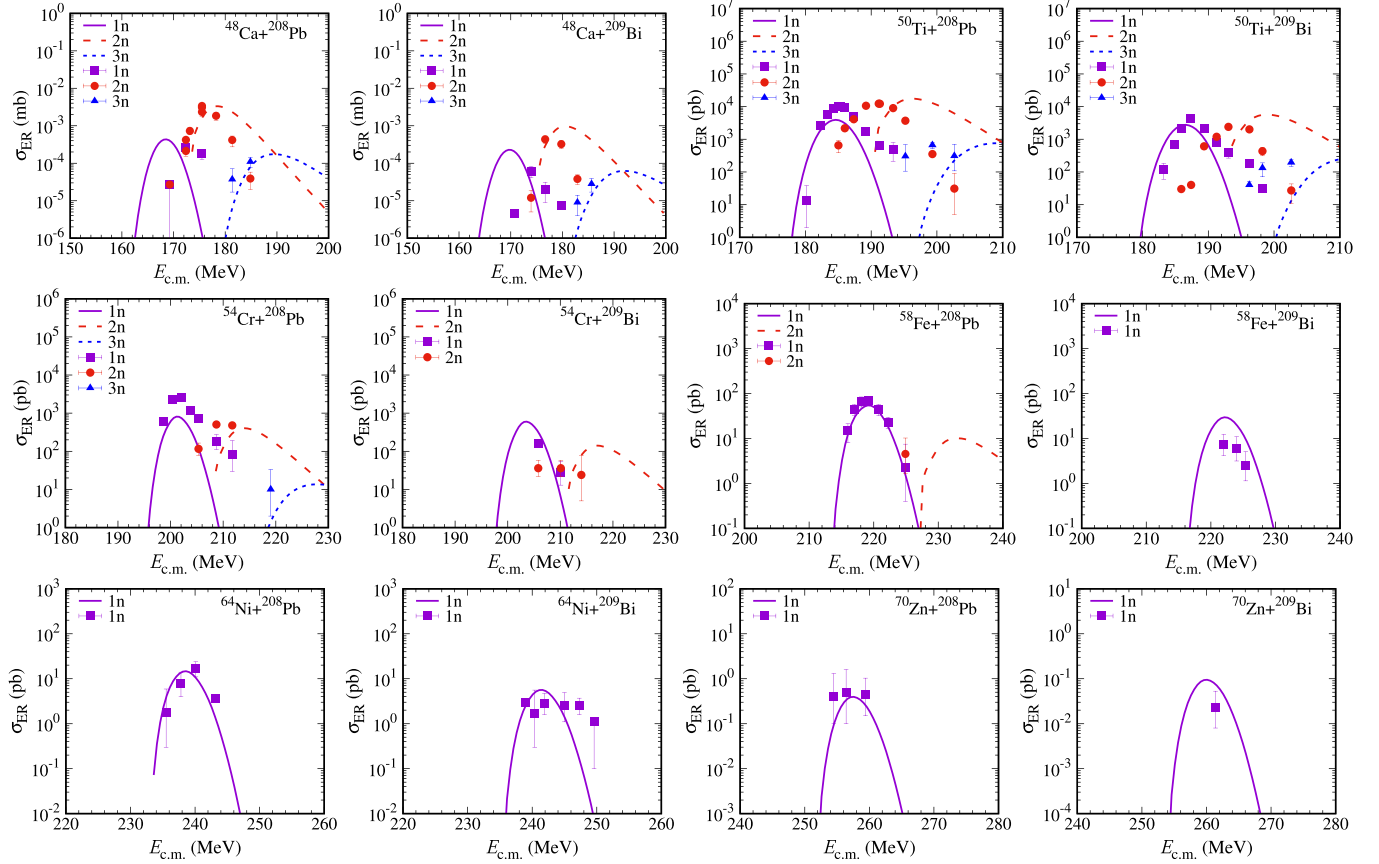


FIG. 2. Evaporation-residue cross sections as a function of the incident energy in the center-of-mass frame for the cold-fusion reactions  $^{48}\text{Ca} + ^{208}\text{Pb}$  [58,59] and  $^{209}\text{Bi}$  [59],  $^{50}\text{Ti} + ^{208}\text{Pb}$  [60] and  $^{209}\text{Bi}$  [60],  $^{54}\text{Cr} + ^{208}\text{Pb}$  [61] and  $^{209}\text{Bi}$  [62],  $^{58}\text{Fe} + ^{208}\text{Pb}$  [61] and  $^{209}\text{Bi}$  [63],  $^{64}\text{Ni} + ^{208}\text{Pb}$  [64,65], and  $^{209}\text{Bi}$  [64,65],  $^{70}\text{Zn} + ^{208}\text{Pb}$  [66,67] and  $^{209}\text{Bi}$  [2]. The calculated evaporation-residue cross sections of the  $1n$ ,  $2n$ , and  $3n$  channels are denoted by the solid, dashed, and dotted curves, respectively.

In the present work,  $B_n$  is calculated by the WS mass formula [55,56].

### III. RESULTS AND DISCUSSION

Based on our previously established methods for calculating the capture cross sections and the survival probability [35,39], we adopt the formula (6) with the three parameters for a systematic investigation of the ER cross sections of the reactions leading to SHN. For calculating the capture cross sections, there are no free parameters in the ECC model. For calculating the survival probability, the shell correction energy  $B_f^{\text{mic}}$  and the neutron-separation energy  $B_n$  are calculated by the WS mass formula [55,56]. As mentioned above, the parameters of formula (6) are obtained by fitting the ER cross sections of  $^{50}\text{Ti} + ^{209}\text{Bi}$ ,  $^{58}\text{Fe} + ^{208}\text{Pb}$ ,  $^{64}\text{Ni} + ^{208}\text{Pb}$ , and  $^{70}\text{Zn} + ^{208}\text{Pb}$  and keeping the same values for all reactions shown in this section. Finally, we show the predictions of the ER cross sections of some reactions leading to SHN with  $Z = 119$  and  $120$ . Note that the above parameter set in formula (6) for calculating the fusion probability depends on the fission barriers and the neutron separation energies for calculating the survival probabilities of SHN. If one uses a different liquid-drop formula for calculating the fission barriers and the neutron separation energies, the parameters must be readjusted.

#### A. Comparison between the calculated ER cross sections and the data

For the cold-fusion reactions with  $^{208}\text{Pb}$  and  $^{209}\text{Bi}$  as targets and  $^{48}\text{Ca}$  [58,59],  $^{50}\text{Ti}$  [60],  $^{54}\text{Cr}$  [61,62],  $^{58}\text{Fe}$  [61,63],  $^{64}\text{Ni}$  [64,65], and  $^{70}\text{Zn}$  [66,67] as projectiles, the comparisons of the calculated  $\sigma_{\text{ER}}$  with the experimental values are shown in Fig. 2. The calculated ER cross sections of the  $1n$ ,  $2n$ , and  $3n$  channels are denoted by the solid, dashed, and dotted curves, respectively. It can be seen that the experimental data for these reactions are systematically well reproduced. In addition, the calculated maximal ER cross sections of the  $1n$  emission channel are compared with the data of the maximal ER cross sections, which is shown in Fig. 3(a). The solid squares denote the experimental data. The open ones denote the calculated values. It can be seen that the data of the maximal ER cross sections decrease exponentially with increasing the  $Z_{\text{CN}}$  of the synthesized SHN, ranging from  $0.26 \mu\text{b}$  for the reaction  $^{48}\text{Ca} + ^{208}\text{Pb}$  to  $23 \text{fb}$  for  $^{70}\text{Zn} + ^{209}\text{Bi}$ . It seems to be difficult to synthesize SHN with  $Z > 113$  via cold-fusion reactions. Then for these reactions, the calculated  $P_{\text{CN}}$  by the formula (6) with  $E_{\text{CN}}^* = 15 \text{ MeV}$  are also shown as a function of  $Z_{\text{CN}}$  in Fig. 3(b). It can be seen that a rapid decrease in  $P_{\text{CN}}$  ranges from  $0.3$  for  $^{48}\text{Ca} + ^{208}\text{Pb}$  to  $3 \times 10^{-8}$  for  $^{70}\text{Zn} + ^{209}\text{Bi}$ , which is similar to the trend of the data of ER cross sections. It can

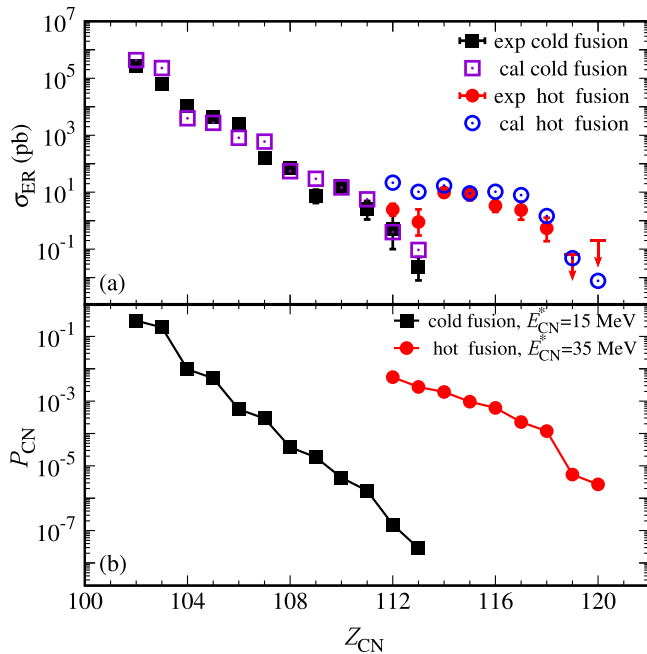


FIG. 3. (a) Maximal ER cross sections for the  $1n$  emission channel of the cold-fusion reactions producing the nuclei with  $Z = 102$ –113 and the hot-fusion reactions leading to the SHN with  $Z = 112$ –118 compared with the calculated maximal ER cross sections. The solid squares and circles denote the experimental data of the cold-fusion reactions and the hot-fusion reactions, respectively. The open ones denote the calculated values. (b) The calculated fusion probabilities for the cold-fusion and the hot-fusion reactions as a function of the charge number  $Z_{CN}$  of the produced SHN. The solid squares denote the results calculated with excitation energy  $E_{CN}^* = 15$  MeV for the cold-fusion reactions. The solid circles denote the results calculated with  $E_{CN}^* = 35$  MeV for the hot-fusion reactions.

be concluded that, for the cold-fusion reactions, the ER cross sections decrease exponentially with increasing the  $Z_{CN}$  due to the rapid decrease in  $P_{CN}$ .

Then the calculated  $P_{CN}$  are also compared with the calculations performed by Adamian *et al.* [18], Feng *et al.* [22], Loveland [20], and Świątecki *et al.* [19], which are shown in Fig. 4. It can be seen that the trend of the curves is similar and the fusion probability decreases rapidly with increasing the  $Z_{CN}$ , while the calculated values of  $P_{CN}$  can differ by two or three orders of magnitude, even though all these models seem able to reasonably fit the measured data of the ER cross sections [11,31,33]. In addition, one can find that the curve of this work locates in the middle of other predictions and is very close to the predictions given by Loveland and Adamian *et al.* It is interesting to note that, in the calculations performed by Loveland and Adamian *et al.*, the ratio  $a_f/a_n$  was taken to be unity [18,20], which consists with the calculated values by the formulas proposed in Ref. [39]. Furthermore, the measured data of  $P_{CN}$  at  $E_{CN}^* = 14.2$  MeV for the reaction  $^{50}\text{Ti} + ^{208}\text{Pb}$  are also shown in Fig. 4 by the open circle. It can be seen that for this reaction the calculated  $P_{CN}$  in this work is consistent with the data.

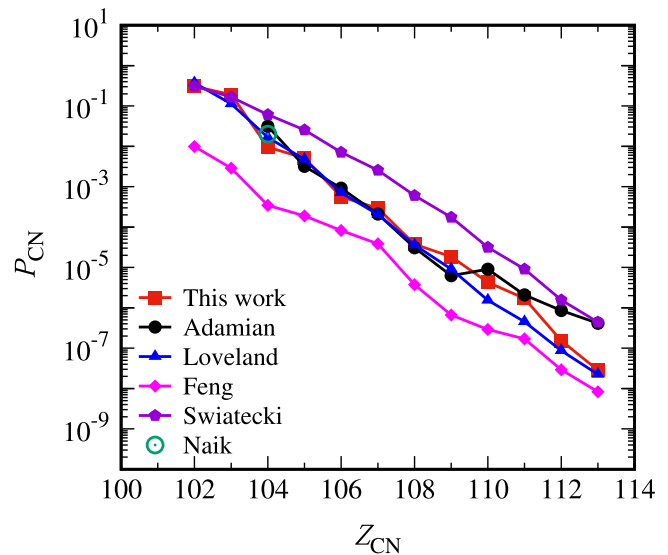


FIG. 4. Comparison of the calculated fusion probabilities for the selected set of the cold-fusion reactions. The theoretical results are taken from Refs. [18–20,22].

With the same parameter set as above, we further investigate the hot-fusion reactions leading to the SHN with  $Z = 112$ –118, i.e.,  $^{48}\text{Ca} + ^{238}\text{U}$ ,  $^{237}\text{Np}$ ,  $^{244}\text{Pu}$ ,  $^{243}\text{Am}$ ,  $^{245,248}\text{Cm}$ ,  $^{249}\text{Bk}$ , and  $^{249}\text{Cf}$ . The comparisons of the calculated  $\sigma_{ER}$  with the experimental data are shown in Fig. 5. The data are taken from Ref. [68]. The calculated ER cross sections of the  $3n$ ,  $4n$ , and  $5n$  channels are denoted by the solid, dashed, and dotted curves, respectively. It can be seen that the experimental data for these reactions are also systematically reproduced. The measured maximal values of ER cross sections for these hot-fusion reactions are compared with the theoretical ones, which are shown in Fig. 3(a). The solid circles denote the experimental data. The open ones denote the calculated values. For the reactions  $^{50}\text{Ti} + ^{249}\text{Bk}$  and  $^{50}\text{Ti} + ^{249}\text{Cf}$  producing SHN with  $Z = 119$  and 120, the cross-section sensitivity levels of 65 and 200 fb [5] are also shown in Fig. 3(a) by the arrows. From  $Z = 112$  to 117, one can find that the experimental cross sections are between 1 and 10 pb. A peak of the ER cross sections appears around  $Z = 114$ . For  $Z > 116$ , the ER cross section decreases almost exponentially as the charge number increases. A similar trend is also found in the calculated ER cross sections for SHN with  $Z = 113$ –118. The calculated  $P_{CN}$  by the formula (6) with  $E_{CN}^* = 35$  MeV are also shown as a function of  $Z_{CN}$  in Fig. 3(b). It can be seen that the calculated  $P_{CN}$  decreases exponentially with increasing the  $Z_{CN}$ .

### B. ER cross sections of SHN with $Z = 119$ and 120

As mentioned above, recently the projectile-target combinations  $^{50}\text{Ti} + ^{249}\text{Bk}$  and  $^{50}\text{Ti} + ^{249}\text{Cf}$  have been used to synthesize the SHN with  $Z = 119$  and 120, and no decay chains consistent with fusion-evaporation reaction products were observed [5]. At a midtarget beam energy of  $E_{lab} = 281.5$  MeV, the cross-section sensitivities are of 65 and 200 fb for  $^{50}\text{Ti} + ^{249}\text{Bk}$  and  $^{50}\text{Ti} + ^{249}\text{Cf}$ , respectively. Here we adopt the formula (6) with the same parameter set to further

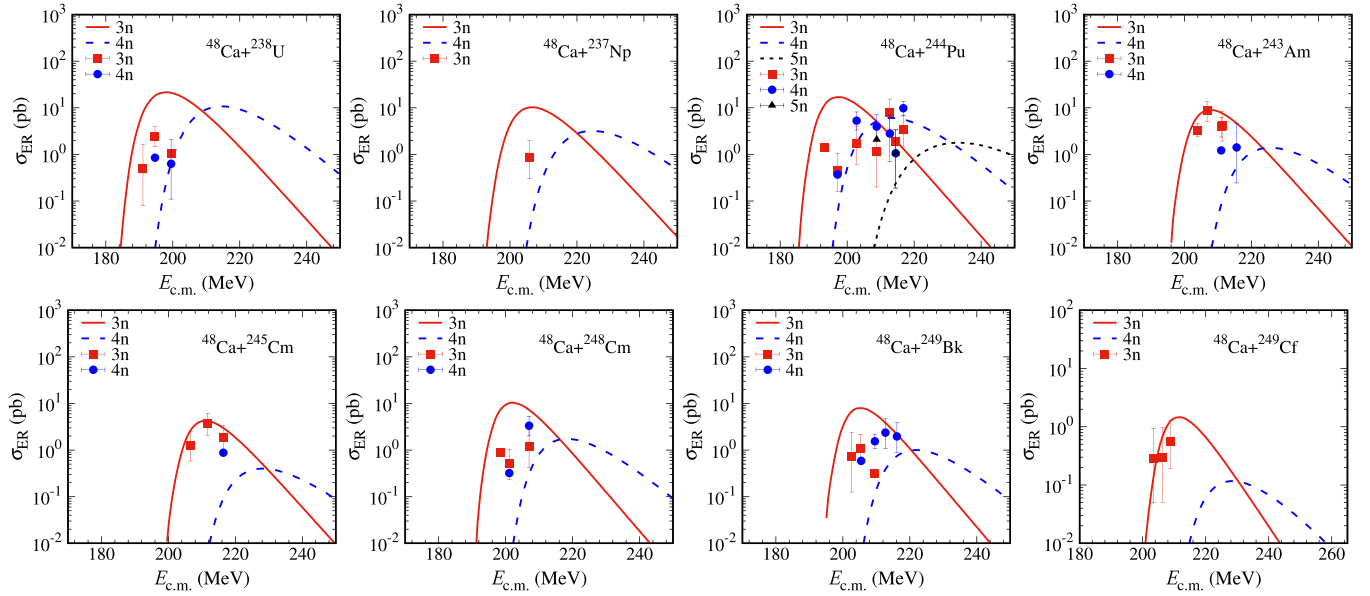


FIG. 5. Evaporation-residue cross sections as a function of the incident energy in the center-of-mass frame for the hot-fusion reactions  $^{48}\text{Ca} + ^{238}\text{U}$ ,  $^{237}\text{Np}$ ,  $^{244}\text{Pu}$ ,  $^{243}\text{Am}$ ,  $^{245,248}\text{Cm}$ ,  $^{249}\text{Bk}$ , and  $^{249}\text{Cf}$ . The calculated evaporation-residue cross sections of the  $3n$ ,  $4n$ , and  $5n$  channels are denoted by the solid, dashed, and dotted curves, respectively. The data are taken from Ref. [68].

investigate the ER cross sections of some hot-fusion reactions producing the SHN with  $Z = 119$  and  $120$ .

Figure 6 shows the calculated ER cross sections for the reactions  $^{45}\text{Sc} + ^{249}\text{Cf}$ ,  $^{50}\text{Ti} + ^{249}\text{Bk}$ ,  $^{51}\text{V} + ^{248}\text{Cm}$ , and  $^{54}\text{Cr} + ^{243}\text{Am}$  producing the SHN with  $Z = 119$ . The solid and dashed curves denote the results for the  $3n$  and  $4n$  emission channels, respectively. The maximal ER cross sections of the  $3n$  and  $4n$  emission channels in the reaction  $^{45}\text{Sc} + ^{249}\text{Cf}$  are 5.47 and 0.72 fb, respectively. For the reaction  $^{50}\text{Ti} + ^{249}\text{Bk}$ , the maximal ER cross sections are 48.2 fb in the  $3n$  emission

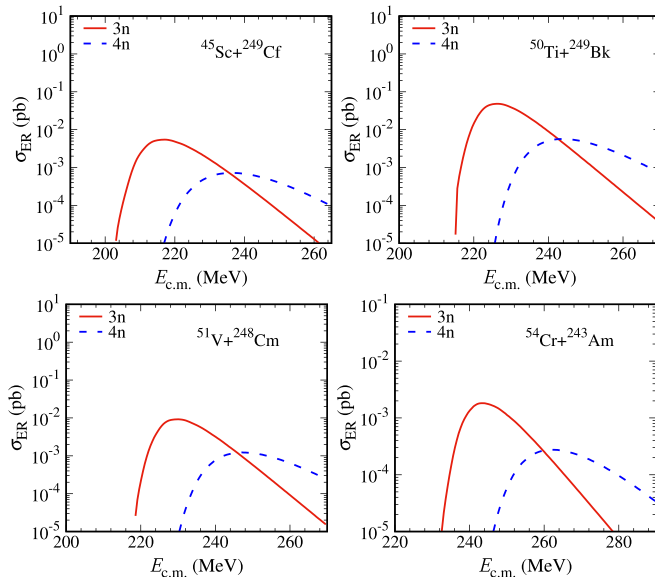


FIG. 6. Evaporation-residue cross sections as a function of the incident energy in the center-of-mass frame for the reactions  $^{45}\text{Sc} + ^{249}\text{Cf}$ ,  $^{50}\text{Ti} + ^{249}\text{Bk}$ ,  $^{51}\text{V} + ^{248}\text{Cm}$ , and  $^{54}\text{Cr} + ^{243}\text{Am}$ . The solid and dashed curves denote the predicted results for the  $3n$  and  $4n$  channels.

channel and 5.67 fb in the  $4n$  emission channel, and the corresponding incident energies are  $E_{c.m.} = 226$  MeV and 243.6 MeV, respectively. In the case of  $^{51}\text{V} + ^{248}\text{Cm}$ , the maximal ER cross section is 9.2 fb in the  $3n$  channel at the incident energy  $E_{c.m.} = 230.1$  MeV. For  $^{54}\text{Cr} + ^{243}\text{Am}$ , the maximal ER cross section is 1.82 fb. Therefore, one can find that the reaction  $^{50}\text{Ti} + ^{249}\text{Bk}$  would be better for synthesizing the superheavy element  $Z = 119$ . The maximal ER cross section is 48.2 fb at the incident energy  $E_{c.m.} = 226$  MeV.

Next we investigate the hot-fusion reactions for the synthesis of isotopes of the SHE with  $Z = 120$ . The ER cross sections for  $^{50}\text{Ti} + ^{249,251}\text{Cf}$ ,  $^{51}\text{V} + ^{249}\text{Bk}$ , and  $^{54}\text{Cr} + ^{248}\text{Cm}$  are shown in Fig. 7. The solid and dashed curves denote the results for the  $3n$  and  $4n$  channels, respectively. It can be seen that in all these four reactions the  $3n$  emission channel gives larger ER cross sections than does the  $4n$  channel. Furthermore, the ER cross sections of the reactions  $^{50}\text{Ti} + ^{249,251}\text{Cf}$  are larger than the other two reactions. For  $^{50}\text{Ti} + ^{249}\text{Cf}$ , the maximal ER cross section is 7.7 fb in the  $3n$  emission channel at the incident energy  $E_{c.m.} = 234.1$  MeV, while for the reaction with  $^{251}\text{Cf}$  as the target, the maximal ER cross section is 17.2 fb at the incident energy  $E_{c.m.} = 230.1$  MeV. For the two reactions  $^{51}\text{V} + ^{249}\text{Bk}$  and  $^{54}\text{Cr} + ^{248}\text{Cm}$ , the maximal ER cross sections are about 1 fb. Therefore, it can be found that the reaction  $^{50}\text{Ti} + ^{249,251}\text{Cf}$  would be the most promising reactions for synthesizing the SHE  $Z = 120$ . The maximal ER cross section is about 10 fb at the incident energies around  $E_{c.m.} = 232$  MeV.

The reactions  $^{50}\text{Ti} + ^{249}\text{Bk}$ ,  $^{50}\text{Ti} + ^{249}\text{Cf}$ ,  $^{54}\text{Cr} + ^{248}\text{Cm}$ , and  $^{58}\text{Fe} + ^{244}\text{Pu}$  producing the isotopes of elements 119 and 120 have been investigated extensively from the theoretical side [9–14,69,70]. For  $^{50}\text{Ti} + ^{249}\text{Bk}$ , the maximal ER cross section ranges from 35 to 600 fb, while for  $^{50}\text{Ti} + ^{249}\text{Cf}$ , the maximal ER cross section ranges from 1.5 to 760 fb. In the present work, the maximal ER cross sections for these two

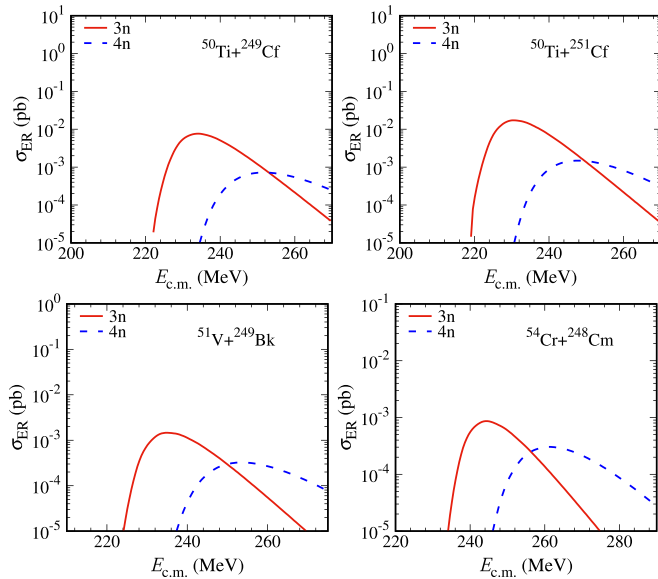


FIG. 7. Evaporation-residue cross sections as a function of the incident energy in the center-of-mass frame for the reactions  $^{50}\text{Ti} + ^{249,251}\text{Cf}$ ,  $^{51}\text{V} + ^{249}\text{Bk}$ , and  $^{54}\text{Cr} + ^{248}\text{Cm}$ . The solid and dashed curves denote the predicted results for the  $3n$  and  $4n$  channels.

reactions are 48.2 and 7.7 fb, respectively. In the case of  $^{54}\text{Cr} + ^{248}\text{Cm}$  and  $^{58}\text{Fe} + ^{244}\text{Pu}$ , the calculated maximal ER cross section falls to a few femtobarns. In this work, for  $^{58}\text{Fe} + ^{244}\text{Pu}$ , the calculated maximal ER cross section is only 0.03 fb. These results show that the projectile-target combinations  $^{50}\text{Ti} + ^{249}\text{Bk}$  and  $^{50}\text{Ti} + ^{249}\text{Cf}$  are considered as the most

promising reactions for the syntheses of the next two SHEs beyond Og.

#### IV. SUMMARY

By using the empirical coupled-channel model for calculating capture cross sections and the statistical model for calculating survival probability, we propose an analytical formula for describing the fusion probability. The cold-fusion and hot-fusion reactions leading to superheavy nuclei have been systematically investigated. For both the cold-fusion and hot-fusion reactions, the measured evaporation-residual cross sections can be reproduced acceptably well by using the formula with the same parameter set. In addition, the evaporation-residue cross sections for some reactions producing elements  $Z = 119$  and  $120$  are studied. The maximal evaporation-residual cross section for  $^{50}\text{Ti} + ^{249}\text{Bk}$  is 48.2 fb at the incident energy  $E_{c.m.} = 226$  MeV. For  $^{50}\text{Ti} + ^{249,251}\text{Cf}$ , the maximal evaporation-residual cross sections are about 10 fb at the incident energies around  $E_{c.m.} = 232$  MeV. In the case of  $^{54}\text{Cr} + ^{248}\text{Cm}$ , the calculated maximal evaporation-residual cross section falls to a few femtobarns. For  $^{58}\text{Fe} + ^{244}\text{Pu}$ , the calculated maximal ER cross section is only 0.03 fb. It is concluded that the projectile-target combinations  $^{50}\text{Ti} + ^{249}\text{Bk}$  and  $^{50}\text{Ti} + ^{249,251}\text{Cf}$  are considered as the most promising reactions for the syntheses of the next two superheavy elements beyond Og.

#### ACKNOWLEDGMENT

This work has been supported by the National Natural Science Foundation of China (Grants No. 11705165, No. 11975209, and No. 11975210).

- [1] S. Hofmann and G. Münzenberg, *Rev. Mod. Phys.* **72**, 733 (2000).
- [2] K. Morita, K. Morimoto, D. Kaji, T. Akiyama, S. Goto, H. Haba, E. Ideguchi, R. Kanungo, K. Katori, H. Koura, H. Kudo, T. Ohnishi, A. Ozawa, T. Suda, K. Sueki, H. Xu, T. Yamaguchi, A. Yoneda, A. Yoshida, and Y. Zhao, *J. Phys. Soc. Jpn.* **73**, 2593 (2004).
- [3] Y. Oganessian, *J. Phys. G: Nucl. Part. Phys.* **34**, R165 (2007).
- [4] Y. T. Oganessian, F. S. Abdullin, P. D. Bailey, D. E. Benker, M. E. Bennett, S. N. Dmitriev, J. G. Ezold, J. H. Hamilton, R. A. Henderson, M. G. Itkis, Y. V. Lobanov, A. N. Mezentsev, K. J. Moody, S. L. Nelson, A. N. Polyakov, C. E. Porter, A. V. Ramayya, F. D. Riley, J. B. Roberto, M. A. Ryabinin *et al.*, *Phys. Rev. Lett.* **104**, 142502 (2010).
- [5] J. Khuyagbaatar, A. Yakushev, C. E. Düllmann, D. Ackermann, L.-L. Andersson, M. Asai, M. Block, R. A. Boll, H. Brand, D. M. Cox, M. Dasgupta, X. Derks, A. Di Nitto, K. Eberhardt, J. Even, M. Evers, C. Fahlander, U. Forsberg, J. M. Gates, N. Gharibyan *et al.*, *Phys. Rev. C* **102**, 064602 (2020).
- [6] S. Hofmann, S. Heinz, R. Mann, J. Maurer, G. Münzenberg, S. Antalic, W. Barth, H. G. Burkhard, L. Dahl, K. Eberhardt, R. Grzywacz, J. H. Hamilton, R. A. Henderson, J. M. Kenneally, B. Kindler, I. Kojouharov, R. Lang, B. Lommel, K. Miernik, D. Miller *et al.*, *Eur. Phys. J. A* **52**, 180 (2016).
- [7] Y. T. Oganessian, V. K. Utyonkov, Y. V. Lobanov, F. S. Abdullin, A. N. Polyakov, R. N. Sagaidak, I. V. Shirokovsky, Y. S. Tsyganov, A. A. Voinov, A. N. Mezentsev, V. G. Subbotin, A. M. Sukhov, K. Subotic, V. I. Zagrebaev, S. N. Dmitriev, R. A. Henderson, K. J. Moody, J. M. Kenneally, J. H. Landrum, D. A. Shaughnessy *et al.*, *Phys. Rev. C* **79**, 024603 (2009).
- [8] S. Hofmann, D. Ackermann, S. Antalic, V. F. Comas, S. Heinz, J. A. Heredia, F. P. Hessberger, J. Khuyagbaatar, B. Kindler, I. Kojouharov, M. Leino, B. Lommel, R. Mann, K. Nishio, A. G. Popeko, S. Saro, J. Uusitalo, M. Venhart, A. V. Yeremin, GSI Scientific Report 2009-1 (GSI, 2019), p. 131, <http://repository.gsi.de/record/53523>.
- [9] V. Zagrebaev and W. Greiner, *Phys. Rev. C* **78**, 034610 (2008).
- [10] N. Wang, J. Tian, and W. Scheid, *Phys. Rev. C* **84**, 061601(R) (2011).
- [11] L. Zhu, W.-J. Xie, and F.-S. Zhang, *Phys. Rev. C* **89**, 024615 (2014).
- [12] N. Wang, E.-G. Zhao, W. Scheid, and S.-G. Zhou, *Phys. Rev. C* **85**, 041601(R) (2012).
- [13] Z.-H. Liu and J.-D. Bao, *Phys. Rev. C* **84**, 031602(R) (2011).
- [14] X. J. Bao, Y. Gao, J. Q. Li, and H. F. Zhang, *Phys. Rev. C* **92**, 034612 (2015).
- [15] N. V. Antonenko, E. A. Cherepanov, A. K. Nasirov, V. P. Permjakov, and V. V. Volkov, *Phys. Lett. B* **319**, 425 (1993).

- [16] E. A. Cherepanov, V. V. Volkov, N. V. Antonenko, V. P. Permjakov, and A. K. Nasirov, *Nucl. Phys. A* **583**, 165 (1995).
- [17] G. G. Adamian, N. V. Antonenko, W. Scheid, and V. V. Volkov, *Nucl. Phys. A* **627**, 361 (1997).
- [18] G. G. Adamian, N. V. Antonenko, and W. Scheid, *Nucl. Phys. A* **678**, 24 (2000).
- [19] W. J. Świątecki, K. Siwek-Wilczyńska, and J. Wilczyński, *Phys. Rev. C* **71**, 014602 (2005).
- [20] W. Loveland, *Phys. Rev. C* **76**, 014612 (2007).
- [21] Z. Liu and J. Bao, *Sci. China G* **49**, 641 (2007).
- [22] Z.-Q. Feng, G.-M. Jin, J.-Q. Li, and W. Scheid, *Phys. Rev. C* **76**, 044606 (2007).
- [23] C. Wang, J. Zhang, Z. Z. Ren, and C. W. Shen, *Phys. Rev. C* **82**, 054605 (2010).
- [24] L. Zhu, Z.-Q. Feng, C. Li, and F.-S. Zhang, *Phys. Rev. C* **90**, 014612 (2014).
- [25] X. J. Bao, Y. Gao, J. Q. Li, and H. F. Zhang, *Phys. Rev. C* **91**, 011603(R) (2015).
- [26] V. I. Zagrebaev, *Phys. Rev. C* **64**, 034606 (2001).
- [27] Z.-Q. Feng, G.-M. Jin, F. Fu, and J.-Q. Li, *Nucl. Phys. A* **771**, 50 (2006).
- [28] G. Mandaglio, G. Giardina, A. K. Nasirov, and A. Sobiczewski, *Phys. Rev. C* **86**, 064607 (2012).
- [29] N. V. Antonenko, E. A. Cherepanov, A. K. Nasirov, V. P. Permjakov, and V. V. Volkov, *Phys. Rev. C* **51**, 2635 (1995).
- [30] R. Smolańczuk, *Phys. Rev. C* **81**, 067602 (2010).
- [31] H. Lü, D. Boilley, Y. Abe, and C. Shen, *Phys. Rev. C* **94**, 034616 (2016).
- [32] K. Wen, F. Sakata, Z.-X. Li, X.-Z. Wu, Y.-X. Zhang, and S.-G. Zhou, *Phys. Rev. Lett.* **111**, 012501 (2013).
- [33] R. S. Naik, W. Loveland, P. H. Sprunger, A. M. Vinodkumar, D. Peterson, C. L. Jiang, S. Zhu, X. Tang, E. F. Moore, and P. Chowdhury, *Phys. Rev. C* **76**, 054604 (2007).
- [34] A. K. Nasirov, G. Mandaglio, G. Giardina, A. Sobiczewski, and A. I. Muminov, *Phys. Rev. C* **84**, 044612 (2011).
- [35] B. Wang, K. Wen, W.-J. Zhao, E.-G. Zhao, and S.-G. Zhou, *At. Data Nucl. Data Tables* **114**, 281 (2017).
- [36] B. Wang, W. Zhao, E. Zhao, and S. Zhou, *Sci. China: Phys., Mech. Astron.* **59**, 642002 (2016).
- [37] B. Wang, W. Zhao, E. Zhao, and S. Zhou, *Nucl. Phys. Rev.* **34**, 539 (2017).
- [38] N. Wang, K. Zhao, W. Scheid, and X. Wu, *Phys. Rev. C* **77**, 014603 (2008).
- [39] B. Wang, Z.-Y. Yue, and W.-J. Zhao, *Phys. Rev. C* **103**, 034605 (2021).
- [40] D. L. Hill and J. A. Wheeler, *Phys. Rev.* **89**, 1102 (1953).
- [41] L.-L. Li, S.-G. Zhou, E.-G. Zhao, and W. Scheid, *Int. J. Mod. Phys. E* **19**, 359 (2010).
- [42] B. Wang, W.-J. Zhao, P. R. S. Gomes, E.-G. Zhao, and S.-G. Zhou, *Phys. Rev. C* **90**, 034612 (2014).
- [43] B. Wang, W.-J. Zhao, A. Diaz-Torres, E.-G. Zhao, and S.-G. Zhou, *Phys. Rev. C* **93**, 014615 (2016).
- [44] L. Guo, C. Shen, C. Yu, and Z. Wu, *Phys. Rev. C* **98**, 064609 (2018).
- [45] G. G. Adamian, N. V. Antonenko, S. P. Ivanova, and W. Scheid, *Phys. Rev. C* **62**, 064303 (2000).
- [46] A. S. Zubov, G. G. Adamian, N. V. Antonenko, S. P. Ivanova, and W. Scheid, *Phys. Rev. C* **65**, 024308 (2002).
- [47] A. S. Zubov, G. G. Adamian, N. V. Antonenko, S. P. Ivanova, and W. Scheid, *Phys. Rev. C* **68**, 014616 (2003).
- [48] V. Weisskopf and D. Ewing, *Phys. Rev.* **57**, 472 (1940).
- [49] N. Bohr and J. A. Wheeler, *Phys. Rev.* **56**, 426 (1939).
- [50] A. S. Zubov, G. G. Adamian, N. V. Antonenko, S. P. Ivanova, and W. Scheid, *Eur. Phys. J. A* **23**, 249 (2004).
- [51] C. Xia, B. Sun, E. Zhao, and S. Zhou, *Sci. China: Phys., Mech. Astron.* **54**, 109 (2011).
- [52] W. Reisdorf, *Z. Phys. A* **300**, 227 (1981).
- [53] S. Cohen and W. J. Świątecki, *Ann. Phys.* **22**, 406 (1963).
- [54] W. D. Myers and W. J. Świątecki, *Ann. Phys.* **84**, 186 (1974).
- [55] N. Wang, M. Liu, and X. Wu, *Phys. Rev. C* **81**, 044322 (2010).
- [56] N. Wang, Z. Liang, M. Liu, and X. Wu, *Phys. Rev. C* **82**, 044304 (2010).
- [57] J. D. Jackson, *Can. J. Phys.* **34**, 767 (1956).
- [58] A. J. Pacheco, J. O. Fernández Niello, D. E. DiGregorio, M. di Tada, J. E. Testoni, Y. Chan, E. Chávez, S. Gazes, E. Plagnol, and R. G. Stokstad, *Phys. Rev. C* **45**, 2861 (1992).
- [59] H. W. Gäggeler, D. T. Jost, A. Türler, P. Armbruster, W. Bröchle, H. Folger, F. P. Heßberger, S. Hofmann, G. Münzenberg, V. Ninov, W. Reisdorf, M. Schädel, K. Sümmerer, J. V. Kratz, U. Scherer, and M. E. Leino, *Nucl. Phys. A* **502**, 561 (1989).
- [60] F. Heßberger, S. Hofmann, D. Ackermann, V. Ninov, M. Leino, G. Münzenberg, S. Saro, A. Lavrentev, A. Popeko, A. Yeremin, and C. Stodel, *Eur. Phys. J. A* **12**, 57 (2001).
- [61] S. Hofmann, F. Heßberger, D. Ackermann, S. Antalic, P. Cagarda, B. Kindler, P. Kuusiniemi, M. Leino, B. Lommel, O. Malyshev, R. Mann, G. Münzenberg, A. Popeko, S. Šaro, B. Streicher, and A. Yeremin, *Nucl. Phys. A* **734**, 93 (2004).
- [62] G. Münzenberg, S. Hofmann, F. P. Heßberger, W. Reisdorf, K. H. Schmidt, J. H. R. Schneider, P. Armbruster, C. C. Sahn, and B. Thuma, *Z. Phys. A* **300**, 107 (1981).
- [63] G. Münzenberg, W. Reisdorf, S. Hofmann, Y. Agarwal, F. Heßberger, K. Poppensieker, J. Schneider, W. Schneider, K.-H. Schmidt, H.-J. Schött, and P. Armbruster, *Z. Phys. A* **315**, 145 (1984).
- [64] S. Hofmann, V. Ninov, F. Heßberger, P. Armbruster, H. Folger, G. Münzenberg, H. Schött, A. Popeko, A. Yeremin, A. Andreyev, S. Saro, R. Janik, and M. Leino, *Z. Phys. A* **350**, 281 (1995).
- [65] K. Morita, K. Morimoto, D. Kaji, S. Goto, H. Haba, E. Ideguchi, R. Kanungo, K. Katori, H. Koura, H. Kudo, T. Ohnishi, A. Ozawa, J. Peter, T. Suda, K. Sueki, I. Tanihata, F. Tokanai, H. Xu, A. Yeremin, A. Yoneda *et al.*, *Nucl. Phys. A* **734**, 101 (2004).
- [66] S. Hofmann, F. Heßberger, D. Ackermann, G. Münzenberg, S. Antalic, P. Cagarda, B. Kindler, J. Kojouharova, M. Leino, B. Lommel, R. Mann, A. Popeko, S. Reshitko, S. Šaro, J. Uusitalo, and A. Yeremin, *Eur. Phys. J. A* **14**, 147 (2002).
- [67] K. Morita, *Prog. Part. Nucl. Phys.* **62**, 325 (2009).
- [68] Y. T. Oganessian and V. K. Utyonkov, *Rep. Prog. Phys.* **78**, 036301 (2015).
- [69] G. G. Adamian, N. V. Antonenko, and W. Scheid, *Eur. Phys. J. A* **41**, 235 (2009).
- [70] K. Siwek-Wilczyńska, T. Czap, and J. Wilczyński, *Int. J. Mod. Phys. E* **19**, 500 (2010).